Solid State Ionics 179 (2008) 2160–2164

Contents lists available at ScienceDirect

Solid State Ionics

journal homepage: www.elsevier.com/locate/ssi

High ionic conductivity in the pyrochlore-type $Gd_{2-y}La_yZr_2O_7$ solid solution ($0 \le y \le 1$)

J.A. Díaz-Guillén [a], M.R. Díaz-Guillén [a], K.P. Padmasree [a], A.F. Fuentes [a,*], J. Santamaría [b], C. León [b]

[a] Cinvestav-Saltillo, Apartado Postal 663, 25000-Saltillo, Coahuila, Mexico
[b] GFMC, Departamento de Física Aplicada III, Facultad de Física, Universidad Complutense de Madrid, 28040-Madrid, Spain

ARTICLE INFO

Article history:
Received 23 November 2007
Received in revised form 12 June 2008
Accepted 14 July 2008

Keywords:
Pyrochlores
Mechanical milling
Zirconates
Lanthanum
Solid oxide fuel cells

ABSTRACT

As SOFC technology relies at present on La-based perovskites as cathode materials, we have analyzed the effect La-incorporation might have in the ionic conductivity of P-$Gd_2Zr_2O_7$, a pyrochlore-type fast oxygen ion conductor. Single phase powder samples with different La/Gd ratio, were prepared in the pyrochlore-type $Gd_{2-y}La_yZr_2O_7$ solid solution ($0 \le y \le 1$) by mechanically milling stoichiometric mixtures of the corresponding oxides. Electrical conductivity measurements were performed for different compositions by using pressed pellets sintered at 1500 °C, as a function of frequency and temperature. Despite of increasing structural ordering (decreasing number of mobile charge carriers), it was found that oxide–ion conduction at intermediate temperatures is almost La-content independent for $y \le 0.8$ because of decreasing *dc* activation energy (from 1.13 to 0.85 eV). We show that these results can be explained in terms of weaker ion–ion interactions in better ordered structures (i.e., rich La-content), highlighting the importance of structural ordering/disordering in determining the dynamics of mobile oxygen ions.

1. Introduction

Since the widespread commercialization of solid oxide fuel cells (SOFC) is still hampered by different technical challenges caused basically by their high operation temperatures, the search for alternatives to the 8YSZ (8 mol% yttria-stabilized zirconia) oxide–ion conductor is still continuing. Among them, $A_2B_2O(1)_6O(2)$ pyrochlore-type oxides have gained considerable attention because of their remarkable chemical and structural flexibility, adjustables to almost any specific application. Because electroneutrality can be achieved by combining different cation species, their electrical behavior span from that typical of insulators or semiconductors to materials showing high ionic, electronic or mixed conductivity. The present paper deals with the influence of La-incorporation on the electrical properties of P-$Gd_2Zr_2O_7$, the best pyrochlore-type oxygen ion conductor known with σ_{dc} values similar to those of 8YSZ [1].

Gadolinium zirconate is known to exist in two crystal forms, i.e. as a highly disordered pyrochlore (P-$Gd_2Zr_2O_7$) and as an anion deficient fluorite (F-$Gd_2Zr_2O_7$), the latter obtained by annealing the first above 1550 °C and quenching the powders to room-temperature [2]. The fully ordered ideal pyrochlore crystal structure exhibits cubic symmetry (S.G.: $Fd\bar{3}m$) and can be regarded as an ordered anion deficient fluorite (cubic, S.G.: $Fm\bar{3}m$) with twice the cell constant ($a \approx 10$ Å) [3]. The eight-coordinated A-site (16*c* according to the Wyckoff notation) is located at the center of a scalenohedron whereas the six-coordinated B-site (16*d*) is located at the center of a trigonal antiprism. As for the anions, the O(1) occupy the 48*f* site coordinated to two B and two A cations while the O(2) anions occupy the 8*a* site, tetrahedrally coordinated to four A cations. There is in addition another tetrahedral site available for anions in the unit cell, 8*b*, only coordinated to B cations, which is systematically vacant and therefore, ordered pyrochlores are poor ionic conductors. However, defect pyrochlores such as P-$Gd_2Zr_2O_7$ which are intrinsically disordered, show high oxygen ion conduction. Different computer simulation studies have shown that the most stable intrinsic defect in these compounds is an oxygen Frenkel pair consisting of a vacant 48*f* position and an interstitial ion occupying an 8*b* site [4–7]. Hence, the conduction controlling factor is the energy of formation of this defect which is substantially reduced by the presence of disorder on the cation sublattice; i.e. cation disorder increases the similarity between non-equivalent oxygen sites and promotes Frenkel defect-formation. However, compounds showing higher degrees of disorder display also higher activation energies for migration. Thus, the activation energy for oxygen diffusion in P-$Gd_2Zr_2O_7$ is lower than in its fully disordered analogue F-$Gd_2Zr_2O_7$ and in consequence, ionic conductivity is higher in the first. Different attempts of improving the P-$Gd_2Zr_2O_7$ ionic conductivity by aliovalent substitutions at the A and B cation sites (e.g. Ca^{2+} or Sr^{2+} for Gd^{3+}; Al^{3+} or Sc^{3+} for Zr^{4+}), rendered only modest raises if any [8,9]. Neither deviations from stoichiometry (either Gd^{3+} or Zr^{4+} excess) provided better oxygen mobility, and a peak in ionic conductivity is always obtained for the fully stoichiometric P-$Gd_2Zr_2O_7$ [10,11]. Interestingly, pyrochlores showing different degrees of disorder are possible in systems of solid solutions by using the appropriate substitutions on the A- and B-sites, with $A_2B_2O_6(1)O(2)$

* Corresponding author. Cinvestav-Saltillo, Carretera Saltillo-Monterrey km 13.5, 25900-Ramos Arizpe, Coahuila, Mexico. Tel.: +52 8444389600; fax: +52 8444389610.
E-mail address: antonio.fernandez@cinvestav.edu.mx (A.F. Fuentes).

0167-2738/$ – see front matter © 2008 Elsevier B.V. All rights reserved.
doi:10.1016/j.ssi.2008.07.015

pyrochlores becoming anion deficient fluorites $(A,B)_4O_7$ when disorder is complete. In such systems, structural ordering/disordering is strongly correlated with the average A to B cation size ratio, R_A/R_B, with the pyrochlore stability field for zirconates and titanates established in the 1.46 to 1.80 range [12]. As R_A/R_B decreases, disordering increases and consequently, the cation size ratio can be used in pyrochlores to control disorder degree. Extensive experimental work has been carried out in the electrical properties of $Gd_2(B_{1-y}Zr_y)_2O_7$ systems of solid solutions (B=Ti^{4+} or Sn^{4+}) [13–17]. Thus, despite increasing ordering (i.e. decreasing number of mobile charge carriers) as the Ti content increases, bulk *dc* conductivity in the $Gd_2(Ti_{1-y}Zr_y)_2O_7$ series remains almost constant for $y \geq 0.4$ because of decreasing activation energy [13]. The situation in the tin-containing series is different because both cations have similar ionic radii and hence, Sn^{4+} substitution for Zr^{4+} does not have any noticeable effect on ordering. However, oxygen mobility decreases with increasing Sn content which has been related with the lower polarizability of its electronic cloud when compared with that of Zr [16]. Electrical properties have been also investigated in Nd and Sm substituted F-$Gd_2Zr_2O_7$ [18]. Thus, a peak in ionic conductivity was observed for the $Gd_{2-y}A_yZr_2O_7$ systems with Nd and Sm contents equal to 0.25 and 0.5 respectively, which was associated with a fluorite-to-pyrochlore phase transition on doping.

As SOFC technology relies at present on La-based perovskites as cathode materials, it would be interesting to analyze the effect La might have in the ionic conductivity of P-$Gd_2Zr_2O_7$. In fact, SOFC's performance is significantly affected by the presence of insulating materials such as $La_2Zr_2O_7$ and $SrZrO_3$, at the 8YSZ/$La_{1-x}Sr_xMnO_3$ interface because of solid state reactions taking place during co-sintering or even during long-term operation. As we have already shown, La-incorporation into the fluorite-type F-$Gd_2Zr_2O_7$ induces ordering for $y \geq 0.4$ which is also associated with a peak in conductivity [19]. Here we show that by increasing the sintering temperature up to 1500 °C we were able to obtain the pyrochlore-type P-$Gd_{2-y}La_yZr_2O_7$ which are found to display higher ionic conductivities than samples with the same composition but with fluorite structure. Since cation antisite defect-formation enthalpies are estimated to be much higher in the pyrochlore-type lanthanum zirconate than in its gadolinium analogue [4], increasing La-content should promote ordering in the defect pyrochlore P-$Gd_2Zr_2O_7$ and it would be interesting to analyze its effect on the dynamics of mobile oxygen ions and consequently, in conductivity values. Since $La_2Zr_2O_7$ has been shown to be a mixed conductor at high temperatures and oxygen pressures [20], we have limited our study to $Gd_{2-y}La_yZr_2O_7$ samples with $0 \leq y \leq 1$ where electronic contribution should be negligible and *dc* conductivity purely ionic.

2. Experimental

Single phase $Gd_{2-y}La_yZr_2O_7$ materials were prepared by mechanical milling as explained in detail elsewhere [19]. Stoichiometric mixtures of high-purity (>99%) La_2O_3, Gd_2O_3 and ZrO_2 were placed in zirconia containers together with 20 mm diameter zirconia balls as grinding media (balls to powder mass ratio=10:1). Dry mechanical milling was carried out in air in a planetary ball mill by using a rotating disc speed of 350 rpm. Prior to mixing, rare-earth sesquioxides were fired overnight at 900 °C in order to decompose hydroxides, carbonates and oxycarbonates present. Phase evolution on milling was periodically analyzed by using X-ray powder diffraction in a Philips X'pert diffractometer (0.01°/s) using Ni-filtered CuK_α radiation (λ=1.5418 Å) and reactions were considered completed when no traces of the starting reagents were evident by this technique. Electrical properties were measured between 250 and 800 °C, on pellets (10 mm diameter and ~1 mm thickness) obtained by uniaxial pressing of the fine powders prepared by mechanical milling. To increase their mechanical strength and obtain dense samples, pellets were fired at 1500 °C for 6 h (heating and cooling rates 2 °C/min). Electrodes were made by coating opposite faces with platinum paste and firing in air at 800 °C to eliminate organic components and harden the Pt residue. AC impedance measurements were carried out in air by using a Solartron 1260 Frequency Response Analyzer over the 100 Hz to 1 MHz frequency range.

3. Results and discussion

3.1. Sample characterization

As explained elsewhere and irrespective of their La-content [19], all $Gd_{2-y}La_yZr_2O_7$ powder samples prepared by mechanical milling showed very similar XRD patterns resembling that characteristic of fluorite-type compounds with no evidence ever present of the reflections characterizing the long-range ordering of cations and anion vacancies of pyrochlores. Thus, mechanical milling allows the room-temperature preparation of single phase fluorite-type $Gd_{2-y}La_yZr_2O_7$ powders despite of R_A/R_B values well above 1.46 (e.g. 1.54 for $GdLaZr_2O_7$). As we have already shown in the similar $Gd_2(Ti_{1-y}Zr_y)_2O_7$ solid solution [21], post-milling thermal treatments of these metastable powders, facilitates the rearrangement of the cation and anion substructures and the partial relaxation of mechanochemically induced defects. Thus, as Fig. 1 shows, all samples fired at 1500 °C present the superstructure reflections characterizing the pyrochlore crystal structure (i.e. the (111) and (331) peaks at $2\theta \approx 15$ and 37° respectively). No additional reflections belonging to other phases were ever observed. The increasing shift towards low angle (2θ) evident in Fig. 1, is consistent with an increase in cell size in the title solid solution $Gd_{2-y}La_yZr_2O_7$, as La-content increases (R_{Gd}(VIII)=1.053 Å vs. R_{La}(VIII)=1.16 Å [22]).

3.2. Electrical properties

Fig. 2(A) shows a typical log–log representation of the frequency dependence of the real part of the electrical conductivity, $\sigma'(\omega)$, over a range of temperatures for the pyrochlore-type $Gd_{1.7}La_{0.3}Zr_2O_7$ sample selected as representative of the series. As Fig. 2(A) shows, the *ac* conductivity exhibits an almost constant value at low frequencies associated to the *dc* conductivity regime σ_{dc}, and a cross-over to a power-law type dependence at sufficiently high frequencies and/or

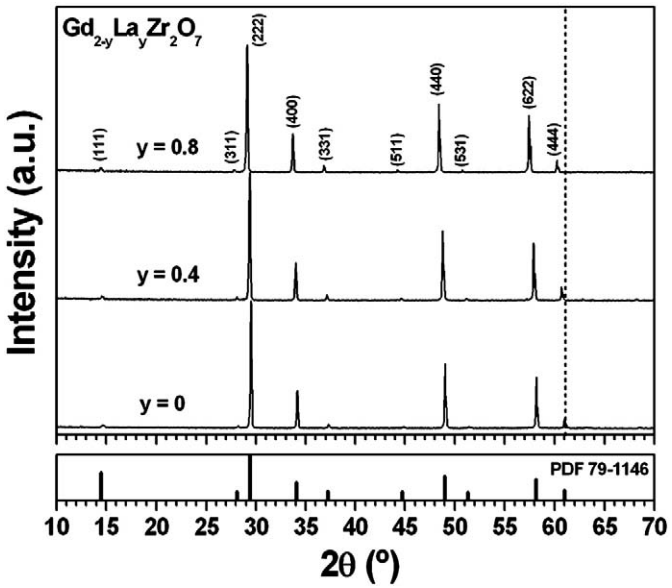

Fig. 1. XRD patterns for selected $Gd_{2-y}La_yZr_2O_7$ samples, prepared by mechanical milling and fired 6 h at 1500 °C; numbers in parenthesis are the Miller indexes of the main reflections of the pyrochlore-type crystal structure. As a reference, the reported XRD pattern of P-$Gd_2Zr_2O_7$ is shown at the bottom. The vertical dashed line is only a guide to the eye shown to emphasize cell changes as lanthanum-content increases.

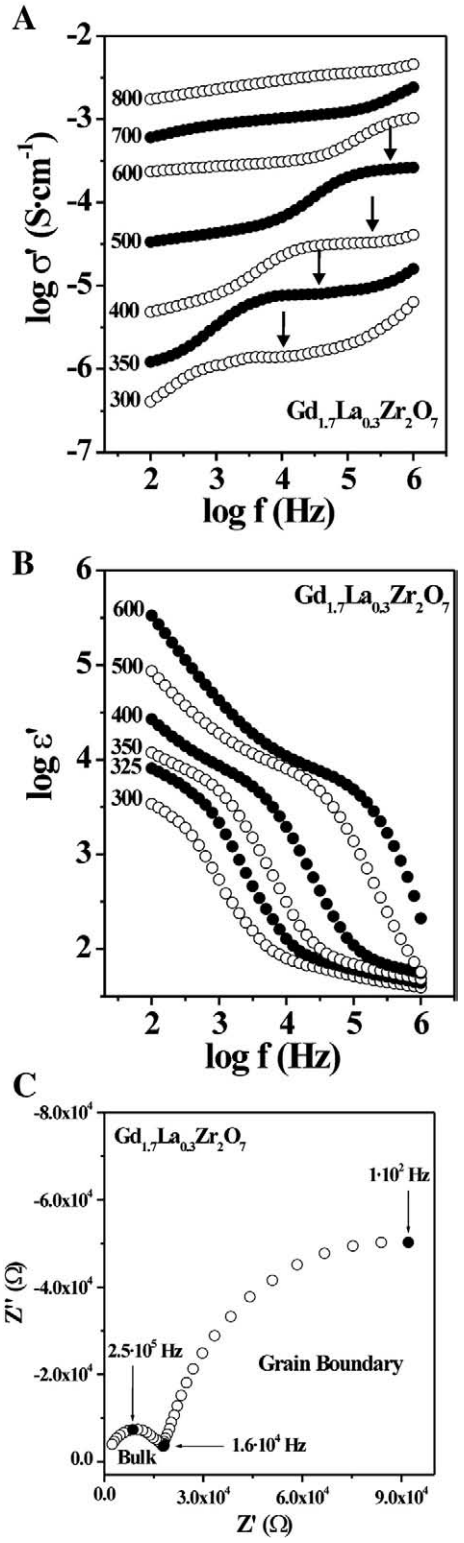

Fig. 2. (A). Log–log representation of the real part of the conductivity vs frequency at several temperatures, for the $Gd_{1.7}La_{0.3}Zr_2O_7$ sample showing the power-law behavior at high frequencies and low temperatures and blocking effects at grain boundaries. Arrows at low and intermediate temperatures are shown to mark the bulk conductivity plateau. (B). Frequency dependence of the real part of the permittivity for the $Gd_{1.7}La_{0.3}Zr_2O_7$ sample at selected temperatures showing blocking effects at grain boundaries and electrodes. (C). Complex impedance plot obtained at 350 °C for $Gd_{1.7}La_{0.3}Zr_2O_7$. Solid circles represent selected frequencies in Hertz.

low temperatures, e.g. in this case evident at 300 and 350 °C. This behavior characterizes the so-called "Universal Dielectric Response" (UDR) proposed by A.K. Jonscher [23] and may be well described by an empirical expression of the type $\sigma'(\omega) \propto \omega^n$, where n is a fractional exponent ($0 \le n \le 1$) which has been linked to correlation effects in the dynamic of hopping ions [24]; thus, the value of n progressively decreases with decreasing interactions among mobile ions ($n=0$ for a Debye-like behavior with completely independent and random ion-hopping). The decrease in conductivity clearly visible at low frequencies and low temperatures, is caused by blocking effects at grain boundaries and shifts towards higher frequencies as temperature raises; i.e., the plateau appearing at lower frequencies is due to the grain boundary contribution to the total conductivity whereas that observed at higher frequencies is due to the bulk contribution.

Fig. 2(B) shows the frequency dependence of the real part of the permittivity for the same sample, also in a log–log representation. Blocking effects at grain boundaries are also observed in this figure shifting to higher frequencies with increasing temperature confirming that conductivity in the sample is basically ionic. Electrode effects are also visible at the highest temperatures as an increase of the apparent permittivity towards low frequencies in Fig. 2(B) and a concomitant decrease of conductivity values in Fig. 2(A). The values of the high frequency permittivity for each sample, ε_∞, were also obtained from this type of graphs and found to be almost independent of temperature and composition, $\varepsilon_\infty = 35 \pm 3$, for the whole series. Grain boundary resistance is also evident in Fig. 2(C) which shows a complex impedance plot obtained for the same $Gd_{1.7}La_{0.3}Zr_2O_7$ composition, at a measuring temperature of 350 °C. Two main features are then evident: an incomplete arc at low frequencies with capacitance values (about 10^{-9} F cm^{-1}) typical of grain boundary contributions and another one at high frequencies associated with the bulk contribution ($4 \cdot 10^{-12}$ F cm^{-1}). The approximate capacitance values given for the bulk and grain boundary contributions respectively are obtained directly from experimental capacitance values (as determined from the complex admittance of the sample) at frequencies higher and lower than the frequency range where the relaxation in the capacitance is observed (see Fig. 2(B)). In fact, the experimental complex impedance data can be described by using an equivalent circuit model of the form (R_b // Q_b) (R_{gb} // Q_{gb}) where the bulk (b) and grain boundary (gb) contributions are in series, and R and Q in parallel accounts respectively for the corresponding resistance and universal capacitance values of each contribution [23]. Thus, bulk *dc* conductivities for the whole series were easily obtained from experimental data, either from the conductivity value at the plateau observed at medium or high frequencies (see arrows) in log–log σ' vs. frequency plots such as Fig. 2(A) or from complex impedance plots such as Fig. 2(C). For high enough frequencies in complex impedance plots (Nyquist plots) both the real and the imaginary part of the impedance inevitably converge to 0 (see Fig. 2(C)), but there is a plateau in the log–log σ' vs. frequency plots at the frequencies roughly corresponding to the right corner of the bulk semicircle, and at this plateau the real part of the impedance corresponds to the bulk value. The temperature dependence of the *dc* conductivity for the samples under study was analyzed by using an Arrhenius-type law of the form:

$$\sigma_{dc} \cdot T = (\sigma_0) \exp(-E_{dc}/k_B T), \quad (1)$$

where σ_0 and E_{dc} are respectively, the pre-exponential factor (related to the effective number of mobile charge carriers) and the activation energy for the ion conduction process. Fig. 3 shows such representations for selected samples where the lines are least squares best fits to an Arrhenius law confirming that ionic diffusion in the series is thermally activated. Activation energies and pre-exponential factors calculated from the slope and intercept of these linear fits, respectively, are presented in Table 1. As this table shows, La substitution for Gd in P-$Gd_2Zr_2O_7$ decreases the activation energy needed for anion vacancies to migrate, from 1.13 eV for P-$Gd_2Zr_2O_7$ to 0.81 eV for $GdLaZr_2O_7$, but it also decreases the pre-exponential factor as ordering increases. Interestingly, low levels of substitution ($0 \le y \le 0.3$) do not seem to

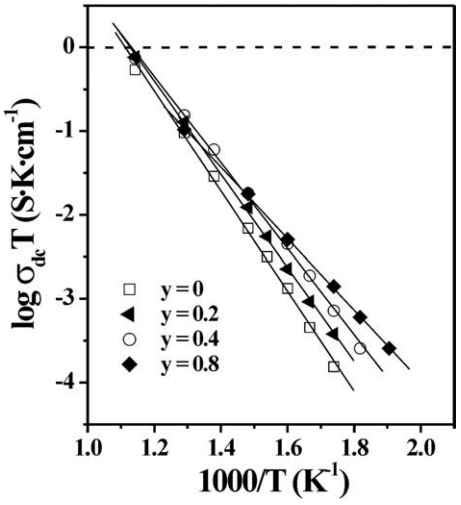

Fig. 3. Arrhenius plots of the *dc* conductivity for selected samples in the $Gd_{2-y}La_yZr_2O_7$ series. Solid lines are the least squares best fits to the experimental data. Error bars are smaller than the size of the symbols.

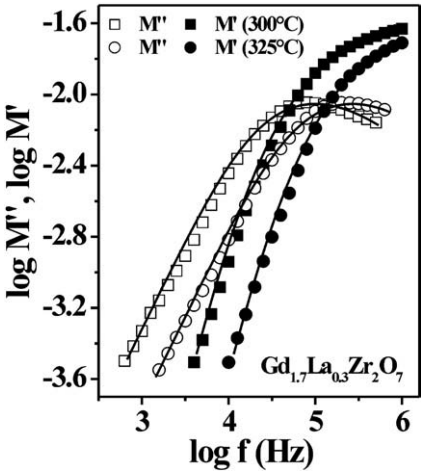

Fig. 4. Frequency dependence of the real (solid symbols) and imaginary parts (open symbols) of the $Gd_{1.7}La_{0.3}Zr_2O_7$ electric modulus at two selected temperatures. Solid lines are best fits according to a KWW relaxation function from which, the exponent *n* might be obtained.

have much effect in ordering since the pre-exponential factor remains almost constant whereas decreasing markedly for $0.4 \le y \le 1$. It is also interesting to compare the ionic conductivity values found in the pyrochlore-type samples of the present study with those of similar samples with the same composition but different (more disordered) fluorite-type structure [19] obtained also by mechanical milling but by sintering at a lower temperature. It can be observed that sintering at 1500 °C instead of at 1200 °C induces higher ordering and that leads to optimized ionic conductivity values, about one order of magnitude higher. As cooperative effects in oxygen hopping dynamics have been shown to be a key factor in determining the activation energy for migration in similar systems [15,25,26], we will proceed now examining the influence of La substitution for Gd in the ion–ion correlations of this solid solution.

An alternative representation of the same electrical relaxation data (i.e. real and imaginary components of the sample impedance) can be made in terms of the time domain by using the complex electric modulus $M^*(\omega)$ which can be expressed by the Fourier transform of the time derivative [27]:

$$M^*(\omega) = \frac{1}{\varepsilon_\infty}\left[1 - \int_0^\infty \left(-\frac{d\Phi}{dt}\right) e^{-j\omega t} dt\right] \quad (2)$$

of the so-called Kohlrausch–Williams–Watts (KWW) relaxation function [28]:

$$\Phi(t) = \exp\left(-(t/\tau)^{1-n}\right), \quad 0 < (1-n) \le 1. \quad (3)$$

where ε_∞ is the dielectric permittivity at high frequencies and τ the characteristic relaxation time of the ion-hopping process which is thermally activated with the same activation energy of the *dc* conductivity. Correspondingly, the time dependence indicated in Eq. (3) is reflected by the spectral shape of the imaginary part of the electric modulus as an asymmetric relaxation peak at a characteristic frequency $\omega_p \approx \tau^{-1}$, which increases with increasing temperature. The fractional exponent *n* defines the power-law dependence of the $M''(\omega)$ above the peak frequency as ω^{n-1}, and consequently the power-law dependence of the real part of the conductivity ($\sigma'(\omega) \propto \omega^n$) at high frequencies which is characteristic of the UDR response. We performed a time-domain analysis in order to obtain a value for the characteristic exponent *n* in each case. Fig. 4 shows the frequency dependence of the real and imaginary parts of the electric modulus for the $Gd_{1.7}La_{0.3}Zr_2O_7$ powder sample at two selected temperatures. Solid lines in the figure are best fits to the experimental data according to Eqs. (2) and (3), from which, the values of the exponent *n* were obtained and observed to be temperature independent for each sample. As expected (see Table 1), the value of *n* was found to remain almost constant for $0 \le y \le 0.3$ whereas decreasing markedly for $y \ge 0.4$. Given the chemical similarity between samples, such a decrease would result from the increasing structural ordering and decreasing concentration of mobile charge carriers.

Interestingly, our results of a concomitant decrease of the activation energy E_{dc} for the *dc* conductivity (see Table 1) and of the

Table 1
dc activation energy, pre-exponential factors and values of *n* obtained for the pyrochlore-type $Gd_{2-y}La_yZr_2O_7$ system

La-content (y in $Gd_{2-y}La_yZr_2O_7$)	Pre-exponential factor (S K cm^{-1})	E_{dc} (eV)	n
0	$1.8 \cdot 10^6$	1.13	0.52
0.2	$1.9 \cdot 10^6$	1.10	0.52
0.3	$1.5 \cdot 10^6$	1.05	0.51
0.4	$6.4 \cdot 10^5$	1.00	0.49
0.8	$3.3 \cdot 10^4$	0.85	0.46
1	$6 \cdot 10^3$	0.81	0.44

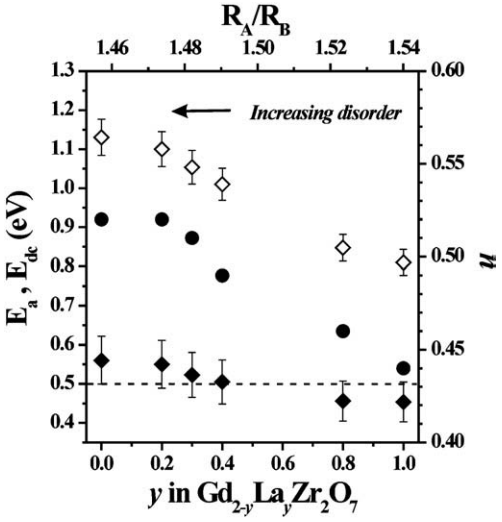

Fig. 5. Values obtained for the activation energy E_{dc} (empty diamonds), the energy barrier $E_a = (1-n)\,E_{dc}$ (solid diamonds) and the exponent *n* for the $Gd_{2-y}La_yZr_2O_7$ series as a function of lanthanum content and the cations size ratio, R_A/R_B. The dashed line represents the average E_a value.

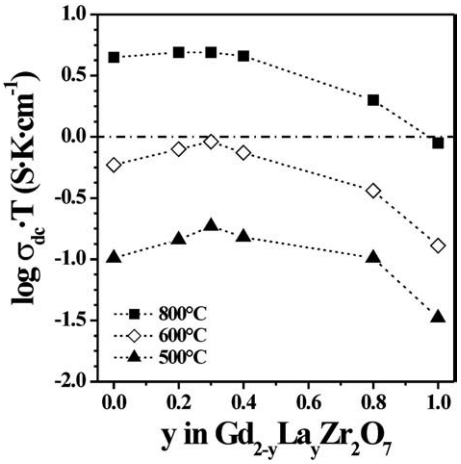

Fig. 6. Bulk *dc* conductivity at three selected temperatures for the pyrochlore-type $Gd_{2-y}La_yZr_2O_7$ solid solution as a function of composition. Error bars are smaller than the size of the symbols.

value of n, with increasing ordering, can be rationalized in terms of the Coupling Model (CM) [24,29–31]. A major result from the CM is that the effective relaxation time τ in Eq. (3) is related to the relaxation time for independent ion-hopping, τ_0, by

$$\tau = \left[t_c^{-n}\tau_0\right]^{1/(1-n)}. \quad (4)$$

For ions vibrating in their cages and hopping to neighboring sites through barriers of energy E_a it is found that $\tau_0(T)=\tau_\infty\exp(E_a/kT)$, with τ_∞ the reciprocal of the attempt frequency of ions. It follows from Eq. (4) that the activation energy for the *dc* conductivity or τ will be larger than the energy barrier and given by the relation

$$E_{dc} = E_a/(1-n). \quad (5)$$

The increase of interactions among the mobile oxygen ions would lead to a higher degree of cooperativity in the ion-hopping process [24,30], that is to a higher value of n and, consequently, to higher activation energies for long-range ionic transport due to the energy penalty that ion–ion interactions impose on the ionic diffusion process. In fact, the activation energy E_a for the barrier that oxygen ions must overcome to hop (independently) between neighboring vacant sites in the pyrochlore-type $Gd_{2-y}La_yZr_2O_7$ series, can thus be estimated according to Eq. (5) by using the experimental values obtained for E_{dc} and n. A value $E_a=0.50\pm0.05$ eV is found, independent of La-content within experimental error (Fig. 5). As it has been shown for similar systems [21,26,32,33], high Gd-contents lead to a higher degree of structural disorder (the size mismatch between cations at the A-site and those located at the B-site decreases) where enhanced ion–ion interactions are expected, and consequently according to the CM, also to higher values of the exponent n as Fig. 5 shows. The more disordered structure fosters ion–ion correlations, and lead to an increase of the energy penalty that these correlations impose on long-range or *dc* ionic conductivity. This explains the increasing difference found between E_{dc} and E_a (larger value of n), the lower the La-content (see Fig. 5).

Finally, Fig. 6 shows the effect of the increasing La-content in the ionic conductivity of the $Gd_{2-y}La_yZr_2O_7$ series, at three selected temperatures. As shown, P-$Gd_2Zr_2O_7$ tolerates lanthanum substitution for Gd without significant reduction in oxygen ion mobility at intermediate temperatures at least for $y\leq0.8$ (σ_{dc} at 800 °C–$5\cdot10^{-3}$ S cm^{-1}). We find of interest now to compare these results with those observed by ourselves when analyzing La-incorporation into fluorite-type $Gd_2Zr_2O_7$ [19] where a peak in ionic conductivity was observed when $y=0.4$ which was associated to a fluorite-to-pyrochlore phase transition. Such phase transition does not exist in the present case because all samples analyzed in this work, present a pyrochlore crystal structure. Interestingly, conductivity in the $Gd_{2-y}La_yZr_2O_7$ solid solution is higher when La replaces Gd in pyrochlore-type $Gd_2Zr_2O_7$ than when doing so in its fluorite analogue [19] which is also in good agreement with previous findings.

4. Conclusions

We have shown that La substitution for Gd in pyrochlore-type $Gd_2Zr_2O_7$ does not affect its ionic conductivity (σ_{dc} at 800 °C–$5\cdot10^{-3}$ S cm^{-1}) at least for $y\leq0.8$ (y in $Gd_{2-y}La_yZr_2O_7$), despite of a decreasing number of mobile oxygen vacancies because of increasing structural ordering. This fact was explained by a marked decrease in the *dc* activation energy for migration with increasing La-content. From the analysis of electrical conductivity relaxation data in terms of Ngai's Coupling Model, we conclude that this behavior is due to the reduction of ion–ion interactions promoted by the more ordered structures in samples with higher La-content.

Acknowledgments

This work has been carried out with financial support from Conacyt (Grant SEP-2003-C02-44075) and the Spanish MCYT (MAT2004-3070-C05).

References

[1] A.J. Burggraaf, T. van Dijk, M.J. Verkerk, Solid State Ionics 5 (1981) 519.
[2] M.P. van Dijk, A.J. Burggraaf, A.N. Cormack, C.R.A. Catlow, Solid State Ionics 17 (1985) 159.
[3] M.A. Subramanian, G. Aravamudan, G.V. Subba Rao, Prog. Solid State Chem. 15 (1985) 55.
[4] L. Minervini, R.W. Grimes, K.E. Sickafus, J. Am. Ceram. Soc. 83 (2000) 1873.
[5] M. Pirzada, R.W. grimes, L. Minervini, J.F. Maguire, K.E. Sickafus, Solid State Ionics 140 (2001) 201.
[6] R.E. Williford, W.J. Weber, R. Devanathan, J.D. Gale, J. Electroceram. 3 (1999) 409.
[7] P.J. Wilde, C.R.A. Catlow, Solid State Ionics 112 (1998) 173.
[8] T. Fournier, J.Y. Nots, J. Muller, J.C. Joubert, Solid State Ionics 15 (1985) 71.
[9] K.V. Govindan Kutty, C.K. Mathews, T.N. Rao, U.V. Varadaju, Solid State Ionics 80 (1995) 99.
[10] T. van Dijk, K.J. de Vries, A.J. Burggraaf, Phys. Status Solidi 58 (1980) 115.
[11] A.V. Shlyakhtina, A.V. Knotko, M.V. Boguslavskii, S. Yu. Stefanovich, I.V. Kolbanev, L.L. Latina, L.G. Shcherbakova, Solid State Ionics 178 (2007) 59.
[12] P.K. Moon, H.L. Tuller, Mater. Res. Soc. Proc. 135 (1989) 149.
[13] M.A. Subramanian, G. Aravamudan, G.V. Subba Rao, Prog. Solid State Chem. 15 (1983) 55.
[14] K.J. Moreno, A.F. Fuentes, J. García-Barriocanal, C. León, J. Santamaría, J. Solid State Chem. 179 (2006) 323.
[15] K.J. Moreno, G. Mendoza-Suárez, A.F. Fuentes, J. García-Barriocanal, C. León, J. Santamaría, Phys. Rev. B 71 (2005) 132301.
[16] T.-H. Yu, H.L. Tuller, Solid State Ionics 86–88 (1996) 177.
[17] P.K. Moon, H.L. Tuller, Solid State Ionics 28–30 (1988) 470.
[18] H. Yamamura, H. Nishino, K. Kakinuma, K. Nomura, Solid State Ionics 158 (2003) 359.
[19] J.A. Díaz-Guillén, M.R. Díaz-Guillén, J.M. Almanza, A.F. Fuentes, J. Santamaría, C. León, J. Phys.: Condens. Matter 19 (2007) 356212.
[20] T.H. Etsell, S.N. Flengas, Chem. Rev. 70 (1970) 339.
[21] K.J. Moreno, A.F. Fuentes, M. Maczka, J. Hanuza, U. Amador, J. Solid State Chem. 179 (2006) 3805.
[22] R.D. Shannon, Acta Crystallogr. A32 (1975) 751.
[23] A.K. Jonscher, Dielectric Relaxation in Solids, Chelsea Dielectric Press, London, 1984.
[24] K.L. Ngai, R.W. Rendell, ACS Symp. Ser. 679 (1997) 45.
[25] K.J. Moreno, A.F. Fuentes, M. Maczka, J. Hanuza, U. Amador, J. Santamaría, C. León, Phys. Rev. B 75 (2007) 184303.
[26] K.J. Moreno, A.F. Fuentes, U. Amador, J. Santamaría, C. León, J. Non-Cryst. Solids 353 (2007) 3947.
[27] K.L. Ngai, C. León, Phys. Rev. B 60 (1999) 9396.
[28] C.T. Moynihan, Solid State Ionics 105 (1998) 175.
[29] K.L. Ngai, C. León, Solid State Ionics 125 (1999) 81.
[30] K.L. Ngai, C. León, Phys. Rev. B 66 (2002) 064308.
[31] K.L. Ngai, C. León, J. Non-Cryst. Solids 315 (2003) 124.
[32] C. Heremans, B.J. Wuensch, J.K. Stalick, E. Prince, J. Solid State Chem. 117 (1995) 108.
[33] B.J. Wuensch, K.W. Eberman, C. Heremans, E.M. Ku, P. Onnerud, E.M.E. Yeo, S.M. Haile, J.K. Stalick, J.D. Jorgensen, Solid State Ionics 129 (2000) 111.